AFRL-RZ-WP-TR-2012-0108

AEROSOL JET DEPOSITION OF CERAMIC THIN FILMS FOR ELECTROCHEMICAL APPLICATIONS

Mary Ayyadurai and Thomas Reitz

Thermal and Electrochemical Branch
Energy/Power/Thermal Division

MARCH 2012
Interim Report

AIR FORCE RESEARCH LABORATORY
PROPULSION DIRECTORATE
WRIGHT-PATTERSON AIR FORCE BASE, OH 45433-7251
AIR FORCE MATERIEL COMMAND
UNITED STATES AIR FORCE

NOTICE AND SIGNATURE PAGE

Using Government drawings, specifications, or other data included in this document for any purpose other than Government procurement does not in any way obligate the U.S. Government. The fact that the Government formulated or supplied the drawings, specifications, or other data does not license the holder or any other person or corporation; or convey any rights or permission to manufacture, use, or sell any patented invention that may relate to them.

This report was cleared for public release by the USAF 88th Air Base Wing (88 ABW) Public Affairs Office (PAO) and is available to the general public, including foreign nationals. Copies may be obtained from the Defense Technical Information Center (DTIC) (http://www.dtic.mil).

AFRL-RZ-WP-TR-2012-0108 HAS BEEN REVIEWED AND IS APPROVED FOR PUBLICATION IN ACCORDANCE WITH THE ASSIGNED DISTRIBUTION STATEMENT.

*//Signature//	//Signature//
RYAN M. MILLER, Ph.D. Chemical Engineer Thermal & Electrochemical Branch Energy/Power/Thermal Division Propulsion Directorate	THOMAS L. REITZ, Ph.D. Branch Chief Thermal & Electrochemical Branch Energy/Power/Thermal Division Propulsion Directorate

This report is published in the interest of scientific and technical information exchange, and its publication does not constitute the Government's approval or disapproval of its ideas or findings.

*Disseminated copies will show "//Signature//" stamped or typed above the signature blocks.

REPORT DOCUMENTATION PAGE

Form Approved
OMB No. 0704-0188

1. REPORT DATE *(DD-MM-YY)*	2. REPORT TYPE	3. DATES COVERED *(From - To)*
March 2012	Interim	01 January 2010 – 30 December 2011

4. TITLE AND SUBTITLE
AEROSOL JET DEPOSITION OF CERAMIC THIN FILMS FOR ELECTROCHEMICAL APPLICATIONS

5a. CONTRACT NUMBER
In-house

5b. GRANT NUMBER

5c. PROGRAM ELEMENT NUMBER
62203F

6. AUTHOR(S)
Mary Ayyadurai and Thomas Reitz

5d. PROJECT NUMBER
3145

5e. TASK NUMBER
01

5f. WORK UNIT NUMBER
314501CK

7. PERFORMING ORGANIZATION NAME(S) AND ADDRESS(ES)
Thermal and Electrochemical Branch (AFRL/RZPS)
Energy/Power/Thermal Division
Air Force Research Laboratory, Propulsion Directorate
Wright-Patterson Air Force Base, OH 45433-7251
Air Force Materiel Command, United States Air Force

8. PERFORMING ORGANIZATION REPORT NUMBER
AFRL-RZ-WP-TR-2012-0108

9. SPONSORING/MONITORING AGENCY NAME(S) AND ADDRESS(ES)
Air Force Research Laboratory
Propulsion Directorate
Wright-Patterson Air Force Base, OH 45433-7251
Air Force Materiel Command
United States Air Force

10. SPONSORING/MONITORING AGENCY ACRONYM(S)
AFRL/RZPS

11. SPONSORING/MONITORING AGENCY REPORT NUMBER(S)
AFRL-RZ-WP-TR-2012-0108

12. DISTRIBUTION/AVAILABILITY STATEMENT
Approved for public release; distribution unlimited.

13. SUPPLEMENTARY NOTES
Report contains color.
PA Case Number: 88ABW-2012-1641; Clearance Date: 22 Mar 2012.

14. ABSTRACT
A novel direct write printing technology namely, aerosol jet printing (AJP) developed by Optomec Inc., has been exploited using suitable processing methods to deposit dense and porous layer components required for the operation of solid oxide fuel cell (SOFC). The research objective of the program is to develop, based on the capabilities of the deposition system, the necessary processing science to reliably deposit SOFC components to have the desired porosity/density for SOFC operation, demonstrate electrode design flexibility for enhanced electrochemical performance, the viability of the novel printing method as a suitable advanced manufacturing method for highly reproducible multi-layered SOFC configurations.

15. SUBJECT TERMS
solid oxide fuel cell, aerosol jet printing, electrochemical process

16. SECURITY CLASSIFICATION OF:			17. LIMITATION OF ABSTRACT:	18. NUMBER OF PAGES	19a. NAME OF RESPONSIBLE PERSON (Monitor)
a. REPORT	b. ABSTRACT	c. THIS PAGE			Stanley Rodrigues
Unclassified	Unclassified	Unclassified	SAR	30	19b. TELEPHONE NUMBER *(Include Area Code)* N/A

Table of Contents

Section **Page**

List of Figures

List of Tables

1 Introduction

Solid oxide fuel cells (SOFCs) offer considerable potential due to their high efficiency, low emissions, fuel flexibility, and their suitability for combined heat and power applications [1,2]. For military needs, SOFCs can serve as field power generators, aircraft auxiliary power units (APUs) and primary power units for small unmanned air vehicles (S-UAV) [3-5]. The advantage of fuel flexibility of SOFCs makes it particularly attractive as a power system for Department of Defense (DoD) applications, where a range of fuel options are available. The ability of SOFCs to use higher hydrocarbons either by direct oxidation or by the use of reformers enables a range of fuels suited for military environments; fuels such as standard gasoline, diesel, JP-8, and fuels synthesized from Fischer-Tropsch process among others. While considerable progress has been made from the materials perspective, SOFC manufacturing methods currently available are limiting. Commonly used methods for fabricating the various cell components are based on wet ceramic processing techniques such as tape casting, screen printing, spray, spin and dip coating for thicker films in the mesoscale range or physical/chemical vapor deposition methods for films in the sub-micron to a few microns in thickness [6]. These methods are not suited for mass manufacture due to limitations in either scale-up or cost.

A novel direct write printing technology namely, Aerosol Jet Printing (AJP) developed by Optomec Inc., has been exploited using suitable processing methods to deposit dense and porous layer components required for the operation of SOFC. Optomec deposition system was delivered under the additional Phase II SBIR program in Aug. 2009. The research objective of the program is to develop, based on the capabilities of the deposition system, the necessary processing science to reliably deposit SOFC components to have the desired porosity/density for SOFC operation, demonstrate electrode design flexibility for enhanced electrochemical performance, the viability of the novel printing method as a suitable advanced manufacturing method for highly reproducible multi-layered SOFC configurations.

1.1 Payoff and Transition Opportunities

Currently, AFRL/RZPS is focused on the advancement of high power density solid oxide fuel cell (SOFC) systems in the 1kW – 10kW range for use as UAV prime power or silent watch vehicle APU applications. SOFC systems offer high efficiencies, fuel flexibility and low audible signature, which makes them particularly attractive for these applications. The realization of high power density SOFCs requires a multi-pronged approach with investments of research efforts in both the materials front and the manufacturing methods. Several groups/laboratories are working on the materials aspect and considerable progress has been made in the achievement of state of the art materials but there is lack of progress in new/novel manufacturing methods. Results of process development work using aerosol jet printing system has highlighted the advantages of this printing based technology to deposit multi-layered fuel cell configurations. The electrode design flexibility with the potential for enhanced electrochemical performance, high reproducibility of component structures and the corresponding device performance, large area printability, and ability to accessorize the system for conformal printing on non-planar substrates are clear advantages over currently available traditional ceramic processing/fabrication methods of screen printing, spray or dip-coating. AFRL/RZPS' efforts in developing the processing science/methods utilizing the

Optomec aerosol jet printing system has excellent payoffs as it complements the progress in UAVs, a rapidly growing area of interest for the Air Force. Moreover, the benefits of the current process development efforts spill into other areas well beyond fuel cells. It can be readily extended to deposit layers in the mesoscale range for different electrochemical and non-electrochemical applications such batteries, capacitors, resistors, transistors, sensors, antennae, etc., critical for military needs.

1.2 Collaborations

RZPS is working closely with Optomec Inc., providing them with the technical input required at the materials processing front, to help engineer/develop suitable accessories for the M^3D deposition system for printing ceramics on tubular SOFC substrates. Since this is an emerging manufacturing method, still in it's initial stage of evolution, the opportunities for collaboration are just opening up. RZPS is currently playing a critical role in the advancement of the technology along with Optomec Inc. for ceramic layer/components manufacturing. We anticipate collaboration with other small business companies and academic institutions as we disseminate the findings of our work. Protonex has expressed an interest in collaboration for deposition of SOFC components for their tubular stacks.

1.3 Organizations Performing Similar Work

As far as materials processing for fuel cells are concerned, ARFL/RZPS is the only group that has currently demonstrated the viability of aerosol jet printing for multi-layer deposition of single components and materials mixing for composite functionally graded materials. It is anticipated that several organizations/groups will build on the initial publications/reports from AFRL.

2 Test Equipment Used

The following test equipments were utilized at different stages of work involving powder characterization, suspension characterization, substrate preparation, layer deposition, thermal treatment, optical and microstructural characterization of layers, fabrication of button cells and electrochemical testing of fuel cells.

2.1 Aerosol Jet Printing

Instrument/Equipment: $M^3D^{®}$ Aerosol Jet™ Deposition System

Location: Building 18, Room 31

DESCRIPTION:

The Deposition subsystem is comprised of different components namely, the deposition head, ultrasonic atomizer and pneumatic atomizers and Process Control Module (PCM). The Motion system, in conjunction with the virtual masking tools (VM T^{TM}) provides coordinated motion on two or three axis (depending on configuration). The AJ™ workstation control software is a visual BASIC-based graphical user interface (GUI) used to

Figure 1: Optomec M^{3}D® aerosol jet deposition system.

control material deposition, substrate motion, and material processing variables. The GUI monitors and controls the substrate position, gas flows and pressures, aerosol preheat temperatures, and substrate temperatures. A vision subsystem comprising of process and alignment cameras facilitate precise positioning of substrates and deposition viewing.

CAPABILITY/PURPOSE:

Deposit/Print films from inks, paste or colloidal suspensions onto substrates (glass, polymeric, ceramic). Typically printed materials are metals and ceramics. Typical substrates range from glass to silicon wafers, polyimide and ceramic substrates depending on the application. Feature sizes from 5μm to a few millimeters with thicknesses ranging from 10nm to several tens of microns can be printed.

EXECUTION

Approach:

Use ultrasonic or pneumatic atomization process to aerosolize inks/pastes or colloidal suspensions of materials to be deposited.

Ultrasonic atomization process

In this application, the ink or other material is held in an atomization vial and positioned over a transducer. The transducer vibrates at ultrasonic frequencies and produces perturbations that eject small droplets from the ink surface. For efficient atomization, the ultrasonic energy must be transferred from the transducer through the coupling fluid and atomization vial to the material. Nitrogen gas or air is used to propel the aerosol. In this process the atomized ink jet is delivered to the Deposition Head where an annular flow is developed between the stream and the sheath gas. The annular flow consists of an atomized ink jet surrounded by the sheath

gas. The purpose of the annular flow is to focus the stream and to prevent impaction of particles onto the walls of deposition tip.

Pneumatic atomization process

The Pneumatic Atomizer uses a high-velocity gas stream to shear a liquid stream into droplets. Compressed gas is expanded through the atomizer nozzle, producing a high velocity jet. As a result of the Bernoulli effect, ink, paste, or other material is drawn from the reservoir into the atomizer nozzle. Subsequently, the high-velocity gas stream breaks the liquid stream into droplets and suspends them in the flow. The high-velocity gas stream, including suspended droplets, exits the nozzle and is impacted on the sidewalls of the atomizer reservoir. Large droplets impact out and drain back into the reservoir while smaller particles remain suspended in the gas. The output from the atomizer is then directed to the Deposition Head.

Success Criteria for deposition by ultrasonic/pneumatic atomization-

(a) Continuous deposition on atomization for tens of minutes
(b) No build-up of atomizer pressure
(c) No frequent nozzle cleaning

2.2 Materials Processing

- Brunauer-Emmet-Till (BET) -ASAP 2020 – measures powder sample surface area and porosity
  NOTE: 3L of liquid nitrogen is required for each test run which is brought for each operation in a safety-approved dewar. Cryogenic gloves and safety goggles are used when handling the liquid nitrogen.
- Pycnometer (AccuPyc 1340) – measures sample absolute density
- Rheometer (RheolabQC) – measures viscosities of prepared ink suspensions
- NiComp ZLS -30 to measures particle size in diluted suspensions
- Muffle furnace – used for sintering of ceramic substrates
  NOTE: furnaces have over-temperature control units
- Ball Mills – processing of ceramic powders
- Uniaxial manual press – densification of ceramic powders for substrates
- Isostatic press – densification of ceramic powders
- Impact mill (Spex SamplePrep 8000M) – processing of ceramic powders
- CO_2 laser cutter – cut ceramic pieces used in testing
  NOTE: 5mW Class 3A CO_2 laser with a Class 1 enclosure and interlocks exhaust system has been installed above required code to vent any exhaust from operation of the laser.

2.3 Microstructural and Electrochemical Characterization

- Optical Microscope/Camera – quick screening of printed surfaces
- FEI Quanta 600 Mk2 FEG-SEM (located in the Materials Directorate-RXLM)- scanning electron microscopy for microstructural assessment

- Dual tube furnace, single clam shell furnace for ramping to cell operation temperatures for two button cells simultaneously
- Solartron multi-channel Cell Test System, 1470E with three channels (three fully independent potentiostat/galvanostats, upgradeable to eight) combined with 1450 series, Frequency Response Analyzer (FRA), capable of a frequency range from 1 mHz to 13 MHz - electrochemical benches for testing multiple cells simultaneously

3 Technical Progress

3.1 Milestones and Lessons Learned

Since acquiring the Optomec $M^3D^{®}$ deposition system, significant progress has been made in process development relating to ceramic suspension formulation, printing various SOFC components, understanding the impact of processing parameters on device performance. Some of the main accomplishments and lessons learnt are listed below:

- Inks suitable for aerosol jet printing of ceramic dense and porous layers for large area SOFC application were developed.

- Printed and subsequently processed electrolyte, Yttria-Stabilized Zirconia (YSZ) was dense and incorporation of this electrolyte in a button SOFC cell gave very stable open circuit voltages of 1.10-1.15 V in the temperature range from 650 -850 ºC.

- Porous composite layers of Ni/YSZ(anode interlayer), and (Strontium doped Lanthanum Manganate (LSM)/YSZ(cathode interlayer) were printed from individually aerosolized inks mixed together on the fly, a feature that enables a wide range of composition variation by simply changing the atomizing/gas flow conditions of the individual components.

- The thickness and microstructure of films produced using aerosol jet printing was highly reproducible resulting in very reproducible electrochemical performance of button cells.

- Button Cells with functionally graded anode interlayer performed better (about 20%) than cells with a non-graded 50/50 wt% Ni-YSZ anode interlayer, demonstrating the advantages of functional gradation, and the potential for enhanced electrochemical performance.

- Parameters such as ink formulation, layer thickness, heat treatment of cathodes were observed to have a significant impact on the cell performance, changing the maximum power density of cells from 200 to 460 mW/cm^2 at 850 ºC, depending on the processing conditions.

- Specialized scanning electron microscopy experiments designed, using low acceleration voltages served as a an effective diagnostic tool to assess material mixing by clearly distinguishing the different phases, Ni and YSZ as well as pores and

percolating and non-percolating Ni in composite layers of Ni/YSZ anode interlayer and LSM and YSZ phases in the cathode interlayer.

3.2 Detailed Technical Progress

The key technical aspects of this work carried out over the course of the reporting period include:

- Ink development and rheological characterization
- Printing of single component dense YSZ electrolyte layer
- Material mixing for printing LSM/YSZ and NiO/YSZ composite layers;
- Functional gradation of anode interlayer, NiO/YSZ
- Microstructure/electrochemical characterization/testing of printed button cells
- Low Voltage SEM measurements to evaluate material mixing
- Cathode, LSM/YSZ optimization
- Large area and miscellaneous printing

3.2.1 Ink development

The electrolyte ink contains Tosoh YSZ (8 mol%), as the active material. The cathode ink contains $(La_{0.8}Sr_{0.2})_{0.98}MnO_3$ (LSM) as the active material. For the composite cathode interlayer, these two inks, LSM and YSZ are mixed during the deposition process. Similarly, NiO and YSZ were mixed for the composite anode interlayer. The solvent used for all inks was a combination of 2-Butanol and α-Terpineol. Three different dispersants were examined: Solsperse 3000 (a penta – (12-hydroxystearic acid) which is a proprietary copolymer with acidic groups), Disperbyk-111 and Dispex A40 (a homopolymer). Polyvinyl butyral (PVB), Butyl Benzyl Phthalate (BBP), Polyalkylene Glycol (PAG) and Ethyl Cellulose (EC) were utilized as binder and plasticizer constituents. Inks were prepared by the addition of powders, to the combination of solvents containing the dispersant. The composition of inks used is shown in Table 1. Based on the results of viscosity and the effect on ink material accumulation at atomizer nozzle, Disperbyk-111 (D111) was chosen as the dispersant in all inks for printing.

Viscosity of inks with dispersant, D111 is shown in Figure 2. The viscosity of YSZ ink with no dispersant, YSZ-0 (see Table 1 for composition) is seen to be 22 mPa*s at lower shear rate (<300 s^{-1}), then decreasing to 20 mPa*s at 300 s^{-1} and thereafter remaining almost constant. The viscosity of YSZ-Sol (YSZ ink with Solsperse 3000 as dispersant, not shown in figure) was much higher than that of YSZ-0 over the entire shear rate range. The viscosity of the YSZ-Sol sample varied from 45 mPa*s at lower shear rates to 38 mPa*s at higher shear rates, (>800 s^{-1}). The viscosity of YSZ- D111 (YSZ ink with Disperbyk-111 as dispersant) was observed to be slightly lower than YSZ-0 in the lower shear rate range, and then seen to converge to that of YSZ-0 at higher shear rates (>650 s^{-1}). The viscosity of YSZ-A40 (not shown in figure) was slightly higher than YSZ-0 in the lower shear rate range, but converges to that of YSZ-0 ink at higher shear rates (>650 s^{-1}). The viscosity of LSM-0 (LSM ink with no dispersant) is seen to be very similar to that of YSZ-0 or YSZ-D111 at very low shear rates up to 100s^{-1}, however, for shear rates greater than 100 s^{-1}, the viscosity is lower than YSZ-0.

In the Newtonian range (region of constant viscosity), the viscosity of LSM-0 is about 15.5 mPa*s. The viscosity of LSM-D111 was observed to be lower than that of LSM-0 over the

Table 1: Composition of Inks.

Constituents for various inks	*YSZ-0 (wt %)*	*YSZ-Sol (wt %)*	*YSZ-D111 (wt %)*	*YSZ-A40 (wt %)*	*LSM-0 (wt %)*	*LSM-D111 (wt %)*	*NiO-D111 (wt%)*
2-Butanol	54.22	53.91	53.91	53.91	54.22	53.91	54.03
α-Terpineol	9.57	9.51	9.5	9.51	9.57	9.51	9.53
YSZ	34.73	34.53	34.53	34.53	0	0	0
NiO	0	0	0	0	0	0	34.6
LSM	0	0	0	0	34.73	34.53	0
Disperbyk-111	0	0	0.56	0	0	0.56	0.56
Solsperse-3000	0	0.56	0	0	0	0	0
Dispex-A40	0	0	0	0.56	0	0	0
Ethyl Cellulose	0.21	0.21	0.21	0.21	0.21	0.21	0
Poly(alkylene glycol)	0.43	0.42	0.42	0.42	0.43	0.42	0.42
Benzyl butyl phthalate	0.43	0.42	0.42	0.42	0.43	0.42	0.42
Poly(vinyl) butyral	0.43	0.42	0.42	0.42	0.43	0.42	0.42

entire shear rate range of interest. The difference is much larger at lower shear rates compared with higher shear rates (> 650 s^{-1}). The viscosity of NiO-D111 is also seen to be shear thinning in the lower shear rate region. It is higher than that of either LSM-D111 or YSZ-D111. Also, some shear thickening can be observed in the higher shear rate region >250s^{-1}.

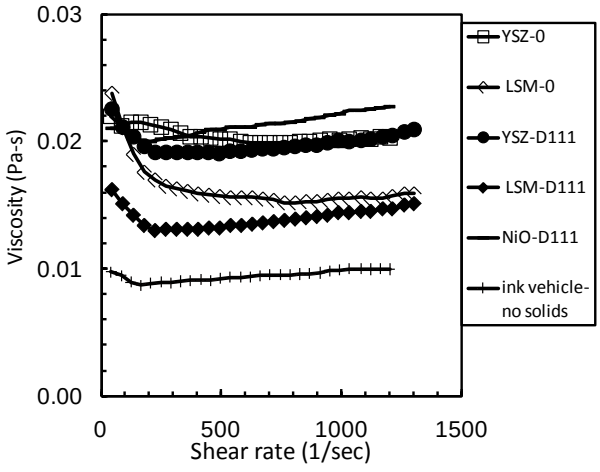

Figure 2: Viscosity of inks.

3.2.2 Printing single component layers

Different patterns generated using AutoCAD® and VMT® are shown in Figure 3a and *d*. The step height of the serpentine/raster fill (a, b and c) was adjusted so that tightly packed fine lines filled the specified rectangular area. Another type of pattern filling was done by using a spiral fill (Fig 3d, e, f.). For this, a decagonal pattern was generated using AutoCAD® polyline segments. The polyline segment width and angles were adjusted using VMT to create a circular pattern that could be filled in a spiraling manner with fine lines of deposit. By changing the values of line spacing, number of print passes, and stage translation speed, films with different wet thicknesses were deposited. Trial runs of these patterns were first deposited on Kapton (shown in fig. 3) tape before using actual substrates.

A commercially supplied anode support was used as substrate. Multiple samples in a single row were held in position by vacuum suction on the platen measuring 6.75x6.75 sq. inches in area. The platen was kept at room temperature (*ca* 26 °C). The pneumatic atomizer vial was filled with YSZ-D111 ink. The ink was atomized using a N_2 gas flow rate of 1500

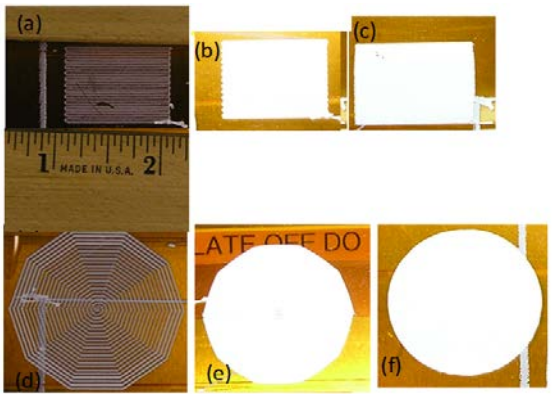

Figure 3: Raster (a,b, and c) pattern and spiral fill patterns (d,e, and f) of YSZ generated using VMT.

sccm. The sheath gas flow (air or N_2) rate of 3000 sccm was maintained. An exhaust gas (air or N_2) flow rate of 1350 sccm was used. The coupons with printed electrolytes were sintered at 1400 °C.

3.2.3 Material mixing for printing composite cathode and anode interlayer

The Aerosol Jet system's dual atomizer configuration is specially designed to allow functional grading of the layers and to permit on-demand material mixing. The capability was used to print the cathode and anode interlayer, which is composed of a mixture of LSM/YSZ and NiO/YSZ, respectively. Instead of the traditional dry mixing/ball milling of the composite materials in order to produce a single ink, here the individually aerosolized inks are mixed together on the fly as they enter the deposition head as shown schematically in Figure 4. Two complete Pneumatic Atomizer Virtual Impactor (PAVI) units feed into a "Y" connector and then into the nozzle head. The two units can be independently controlled such that both, simultaneous or individual use is possible. This feature of material mixing has clear advantages over traditional processing methods, as well as the inkjet method, in that a wide

range of composition variation is readily possible by simultaneously changing the atomizing gas flow conditions of the individual components. In order to determine the relative composition of the material in the composite layers, mass calibration curves were performed. For example, for the cathode interlayer, the deposition rates for YSZ and LSM were initially determined via separate gravimetric measurements using a specialized platen equipped with a weighing scale. Deposition rates for each individual component were determined for a given atomizing flow rate by changing the exhaust flow rate (*i.e.*, changing the amount of atomized material to the deposition head). The sheath gas flow rate was held constant at 3000 sccm. From these calibration curves suitable gas flow conditions for the two components, LSM and YSZ of LSM/YSZ composite were selected such that the two individual atomizers could then be simultaneously operated to output a 1:1 weight ratio of the materials. Following the same procedure NiO and YSZ inks were mixed for the anode interlayer.

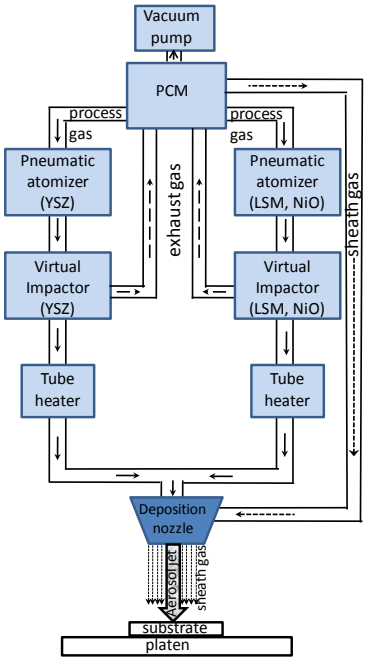

Figure 4: Schematic of dual atomizers for material mixing.

An example of the mass calibration curves in shown in Figure 5 for the cathode interlayer.

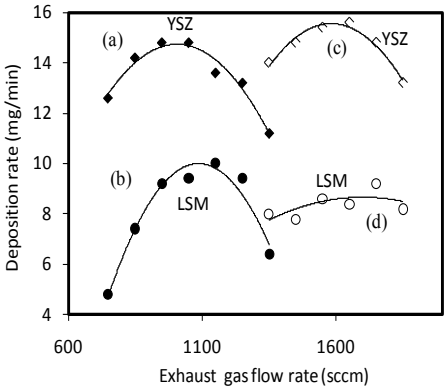

Figure 5 : Mass calibration curves for determination of gas flow conditions for 50/50 cathode interlayer, LSM/YSZ.

The results of deposition rate are shown as a function of exhaust gas flow rate (F_{ex}). Curves *a* and *b* represent the deposition rate for atomizing gas flow rate of 1500 sccm, for YSZ and LSM respectively, and curves *c* and *d* represent the deposition rate for atomizing gas flow rate (F_{at}) of 2000 sccm for YSZ and LSM, respectively. YSZ deposition rate is seen to be at least 1.5 times as high as LSM for F_{at} = 1500 sccm and 2000 sccm. Deposition rate depends on initial particle size/size distribution, dispersion and atomizing conditions. These factors together with the viscosity and surface tension of the suspension determine the size/distribution of atomized droplet and its momentum. Droplets having an optimum size and momentum exit the nozzle. The larger particle size of initial LSM powder is likely one of the contributing factors for the lower deposition rate. For YSZ deposition at F_{at} = 1500 sccm and 2000 sccm, and LSM deposition for F_{at} = 1500 sccm, the trends are similar, with the deposition having a maximum for mist flow rate (mist flow is the difference between atomizing flow and the exhaust flow, i.e., the flow entering the deposition head.) between 350-550 sccm. For mist flow rate above and below this range, the deposition rate decreases. This is possibly due to the dependence of the cross section for deposition on the size distribution of the droplet. For a

given atomizing gas flow rate, as the mist flow increases (decreasing exhaust flow), the deposition increases, reaching a maximum, and then for further increase in mist flow, the number density of droplets having the optimum size and momentum decrease. For LSM deposition at F_{at} = 2000 sccm, the trend is more sluggish, with no clear maximum. The deposition rate is almost independent of exhaust flow rate. Also, it is lower than that for F_{at} = 1500 sccm. This observation suggests that for a given ink (whose rheological properties are determined by the dispersion, size distribution, density, viscosity and surface tension), there is an upper limit of atomizing parameters that play a role in determining the deposition rate. This upper limit shifts depending on the ink characteristics. Thus, by manipulating both, the initial ink characteristics as well as the atomizing conditions, a matrix of deposition rates is possible.

If curve (a) is extrapolated to higher mist flow rate (lower exhaust flow rate), a deposition rate of about 10 mg/min can be obtained. This deposition rate can be obtained for LSM by maintaining the gas flow conditions for the maximum on curve (b). Similarly another flow condition can be established for a 1:1 deposition rate by extrapolating the curve (d) to the higher end of the mist flow rate to intersect curve (b) at its lower end of the mist flow rate. These conditions were experimentally verified, and the following conditions chosen- at F_{at} = 1500 sccm, and F_{ex} = 1400 sccm for YSZ and F_{at} = 2000 sccm, and F_{ex} = 1450 sccm for LSM. Sheath gas flow rate was maintained at 3000 sccm for both LSM and YSZ. Similar gas flow determinations were made for NiO and YSZ. Figure 6 shows the SEM image of the cross-section of the printed cathode interlayer that has been sintered. It can seen that the interlayer is quite porous. However the phase contrast of YSZ and LSM are similar and hence not clearly distinguished.

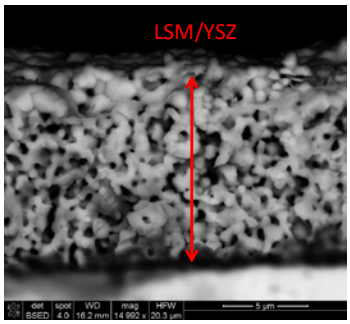

Figure 6: SEM image of the cross section of cathode interlayer, LSM/YSZ.

3.2.4 Microstructure of printed layers and electrochemical performance of button cells

Figure 7a and b (top) shows the SEM image of the surface of typical electrolytes printed with the Optomec system and sintered. It can be seen that electrolyte is dense and well sintered. The grain sizes range from 2-5 μm. Numerous electrolyte films have been generated using this approach with varying thicknesses of 8-33 μm, depending on the type of filling, number of print passes, stage translation speed and fill line width. These films had a high degree of uniformity.

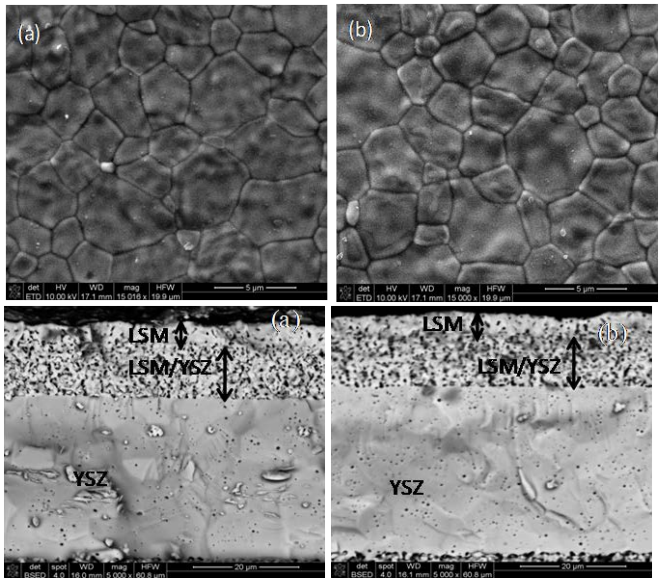

Figure 7: SEM images of the surface of typical YSZ electrolytes (top, a and b) and typical cross sectional view of post tested cells (bottom) having printed electrolyte and cathode layers, LSM/YSZ(interlayer) and LSM (cathode current collecton layer).

Figure 7a and b (bottom) show the post-mortem, cross-sectional SEM images of two prototypical cells with the electrolyte, cathode functional, and cathode current layers aerosol jet printed onto a Ni/YSZ anode support. The two cells are identical in all respects except that the cathode interlayer for cell *a* was printed with a substrate to nozzle distance of 7 mm and the cathode interlayer for cell *b* was printed with a substrate to nozzle distance of 9 mm. Both cells are seen to have a dense electrolyte, about 33 µm thick, and were printed using a spiral fill method consisting of 6 print passes. A porous cathode interlayer (about 11 µm thick) and a thinner, less porous LSM layer (about 4 µm thick) can be seen in the figure above.

Figure 8a, b show the V-I curve of the two cells shown in Figure 7. The cells were

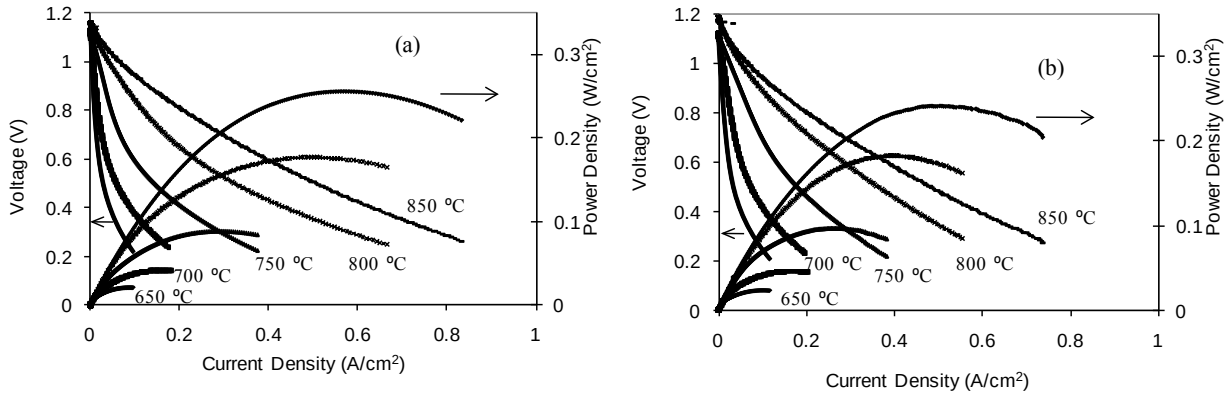

Figure 8: VI plots of cells shown in fig. 7.

tested with hydrogen as the fuel and air as the oxidant. The cells have open circuit voltages (OCV) ranging from 1.16-1.20V, depending on the temperature. As temperature increased from 650°C to 850°C, the current density and power density are seen to increase. The maximum power density at 850˚C for both cells is 250 mW/cm^2. The performance of the cell at lower temperatures, from 650-750ºC, is relatively poor. This is perhaps due to the fact that the cathode layers are sub-optimized. The cathode current collection layer is thin and less porous than the interlayer. The overall lower performance of the cell can be attributed to a very thick electrolyte, lack of anode functional layer, sub-optimum cathode layer thicknesses, and sub-optimum microstructure of the cathode current collection layer. These initial results

are promising and it is anticipated that these inadequacies can be remedied by altering the ink composition and printer processing parameters.

3.2.5 Functional gradation of anode interlayer, x wt % NiO/ (100-x) wt %YSZ

Mass calibration curves described in section 2.3.3 were obtained and suitable gas flow conditions for the atomization of individual inks for the desired compositions x wt % NiO/ (100-x) wt % YSZ, were determined. Two identical sets of anode interlayer, set 1 and set 2 were printed over the printed electrolyte (on a NiO/YSZ support substrate) that was dried at 60 ºC. Each set had 2 different types of NiO/YSZ interlayers as shown schematically in

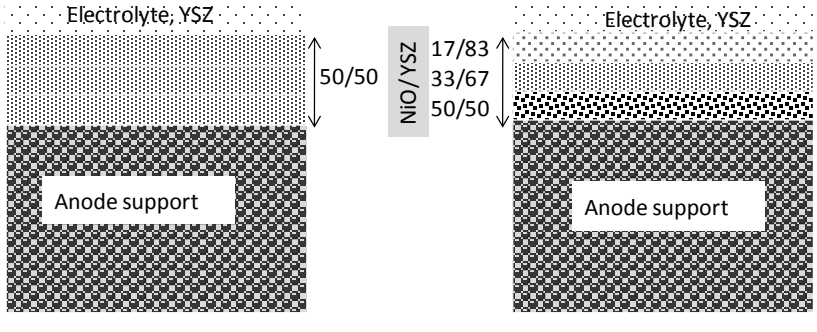

Figure 9: Schematic of anode interlayer designs

Figure 9. Type 1 had 12 print passes of a 50/50 wt % NiO/YSZ and type 2 had a total of 12 print passes with functional gradation in composition along the z-axis. The first 4 print layers/passes (region adjacent to the support substrate) had a composition of wt % 50NiO/50YSZ. The next 4 print passes had a composition of wt % 33 NiO/67 YSZ (4 passes) and the final 4 print passes had a composition of wt % 17 NiO/83 YSZ. In type 2, two different drying procedures were adopted. The first drying procedure consisted of drying the printed anode interlayer by keeping the platen at room temperature (type 2-RT) and the other procedure consisted of drying the interlayer by holding the platen at 60 ºC (type 2-60 ºC). For type 1, the anode interlayer was dried at room temperature. Button cells containing printed electrolyte, schematically depicted printed anode interlayers, and pasted cathode were tested for their electrochemical performance. The VI profiles for these cells are shown in Figure 10. It can be seen from figure 10 that cells with a functionally graded anode interlayer (curves *b* and *c*) perform better than cells with a non graded interlayer (curve *a*). Also the two identical sets show almost identical behavior. Although the overall performance of all cells is poor, nevertheless very clearly elucidates the advantage of functionally graded structures as well as the reproducibility of the printing method.

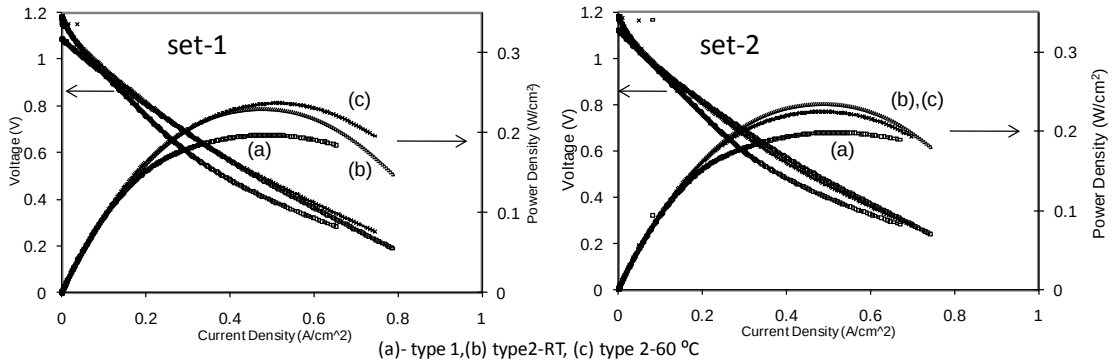

Figure 10: VI plots of two identical sets (set 1 and set 2) of cells with printed electrolyte, anode interlayer designs shown in fig. 9, and pasted cathode layers.

3.2.6 Low voltage scanning electron microscopy (LVSEM) measurements for evaluation of material mixing

While x-ray mapping can differentiate between Ni and YSZ, it takes long acquisition times to collect images that will have a relatively good signal to noise ratio. Also, neither z-contrast imaging with the backscatter electron signal nor x-ray mapping can differentiate between percolating and non-percolating Ni. Further compounding the problem of differentiating between the different phases is the nearly identical backscatter coefficient possessed by the nickel and the YSZ phases (no z- contrast in the backscatter signal). The solution to this analysis problem is the use of low voltage (1 kV) secondary electron imaging of carefully prepared ultra-clean specimens.

Figure 11 (a) shows the secondary electron image (SEI) acquired (on a region in the anode substrate) using a normal 10 kV acceleration voltage and (b) shows the SEI image acquired using 1 kV. It can be seen that in SEI-(a), the YSZ phase is charging intensely, whereas in SEI-(b), two phases can be clearly distinguished; one phase that is grey and smooth and another that is bright and corrugated. To identify the two phases, x-ray mapping was used. Phase identification map constructed from energy dispersive x-ray microanalysis data (green = Ni, Blue = YSZ) shown in fig. 12. Black hi-light boxes indicate the locations of some non-percolating Ni.

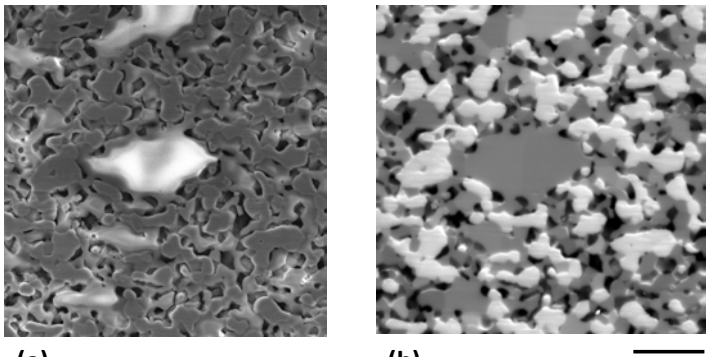

Figure 11: Secondary electron image (SEI) of anode support using (a) 10 kV acceleration and (b) 1 kV acceleration voltage.

Figure 13 shows the low voltage SEI of the cross-section of the electrochemically tested cells (type 1 and type 2-RT) whose anode interlayer design scheme is shown in fig. 9 and electrochemical performance is shown in fig. 10. These images reiterate the reproducibility in layer thickness and microstructure. Both type 1 and type 2 cells have

similar electrolyte and anode interlayer thicknesses. The electrolyte is dense and 12 µm in thickness. Both anode interlayers are 35 µm thick. In type 1, a uniform distribution of Ni and YSZ is seen, while a gradation can be readily seen in type 2 with larger amount of Ni adjacent to the support and increasing YSZ amounts closer to the electrolyte. From the brightness contrast of the Nickel phase, it appears that it is largely percolating. However, a layering effect can be seen in the interlayer region, with features similar to striations of Ni and YSZ suggesting inhomogeneous mixing. Figures 10 and 13, clearly illustrate the advantages of functional gradation of the anode interlayer and ability of the aerosol jet method to deposit

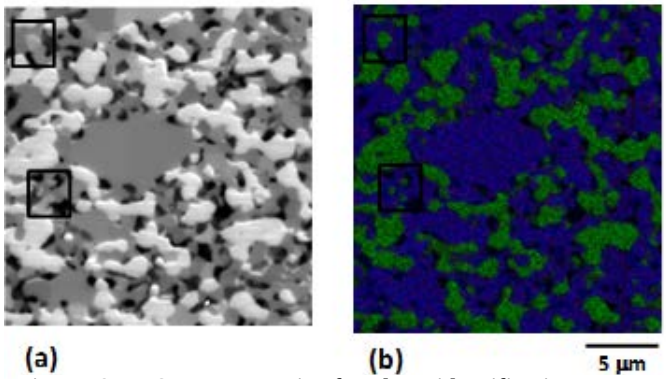

Figure 12: EDS x-ray mapping for phase identification, green-Ni and blue-YSZ.

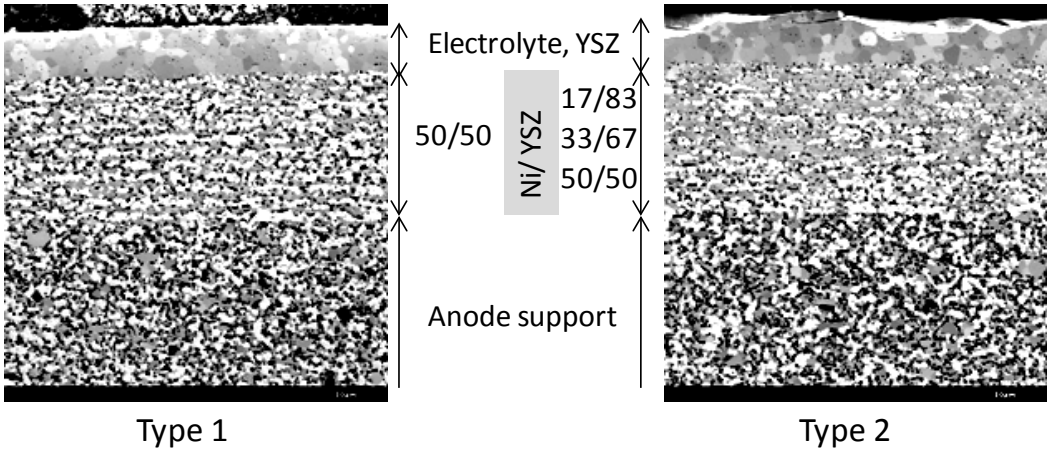

Figure 13: SEI images of post tested cells of set1 (of fig. 10) with anode interlayer scheme shown in fig. 9.

composite/single component layers in a highly reproducible manner. The observation of the layering effect requires further investigation. Alleviation of the layering effect is likely to enhance the performance proportionately in both type 1 and type 2 cells.

Figure 14 shows the LVSEM image of the cathode cell shown in fig. 7a. For clarity sake, magnified images of highlighted regions (a) and (b) are presented. As can be seen from the figure, mixing of LSM and YSZ in the interlayer region is clear. In the anode support, about four phases can be seen; 1) light and dark shades of grey regions that are faceted. This is the YSZ phase. 2) a bright white region, which is the percolating Ni, 3) a lighter white to grey shade of non-faceted isolated regions, which is the non-percolating Ni, and 4) black regions, which correspond to pores. In the dense electrolyte region, grain to grain contrast that arises from electron channeling effects within the crystalline material can be seen. In the LSM/YSZ interlayer, three phases can be seen; 1) a bright white region corresponding to LSM, 2) a grey region corresponding to_YSZ, and 3) a black region corresponding to the pores. The topmost white layer corresponds to LSM. As can be seen from fig. 14, there is good mixing of the two phases, LSM and YSZ. The better mixing at the cathode interlayer

compared to the mixing at the anode interlayer could be due to differences in the suspension properties of the two phases.

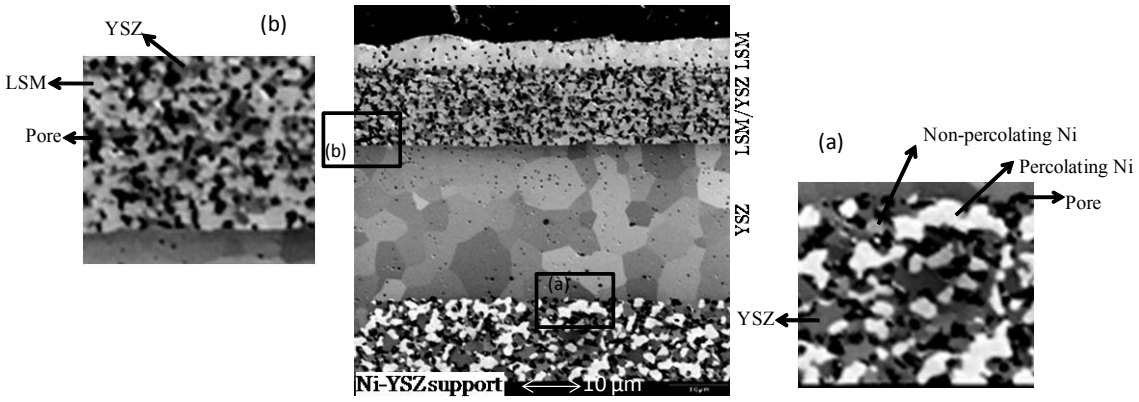

Figure 14. LVSEM image of cross section of a printed cathode cell shown in fig. 7a.

3.2.7 Cathode optimization

In fig. 7, and fig. 14 above, the cathode current collection layer, LSM is observed to be of inadequate thickness (about 4 µm in thickness). In order to increase the thickness, atomizing conditions were chosen that gave higher deposition rates (60 mg/min), and also the number of print passes were increased. Figure 15 shows current/voltage profiles of cells having identically printed and processed electrolyte layer, YSZ and cathode interlayer, LSM/YSZ but differing in the cathode current collection, LSM layer characteristics. Plot (a) shows the cell performance of a cell with 40 print passes of LSM, and plot (b) shows that of a cell with 60 print passes of LSM. The sintering temperature and wt% solids in LSM ink remain the same for both (a) and (b). It can be seen that the cell with 40 print passes of LSM performs better. Plot (c) shows the electrochemical performance of a cell similar to the cell in plot (a) but differing only in the amount of solids wt % in the LSM ink. Clearly the cell in plot (c) performs better than the cell in plot (a). Plot (d) corresponds to a cell identical to that in plot (a) and differing only in the sintering temperature of LSM layer. While the LSM layer in cells of plots (a), (b) and (c) was sintered at 1200 ºC, the LSM layer of cell in plot (d) was sintered at 1150 ºC. These results show the significance of ink composition and processing parameters on the performance of the cell. It must be mentioned that pairs of each type, a), b), c) and d) were tested to assess reproducibility. Typically, very high reproducibility has been achieved with this printing method with no more than 10% difference in power densities within each pair. Also, it is observed that performance of cell (d) matches the performance of a typical pasted cathode cell (6).

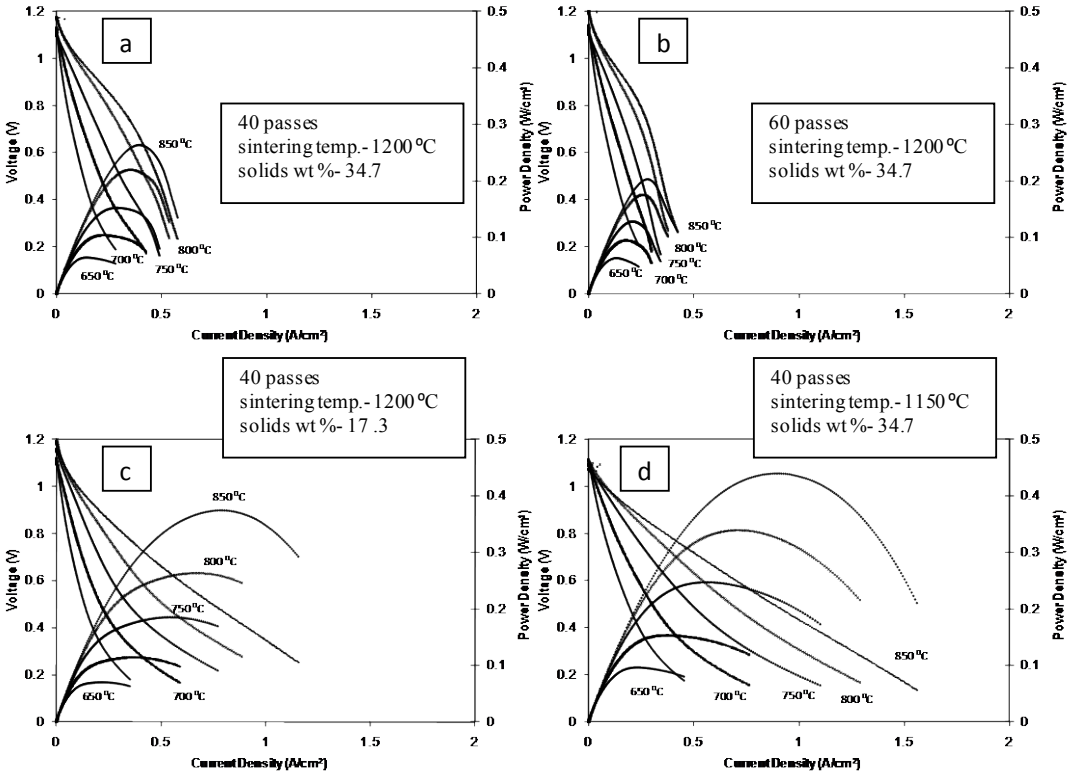

Figure 15: VI Plots of cells with identically processed LSM/YSZ layer and varied LSM layer, (a) 40 passes, solids wt %- 34.7 and sintering temperature- 1200 °C, (b) 60 passes, solids wt %- 34.7 and sintering temperature- 1200 °C, and (c) 40 passes, solids wt %- 17.4 and sintering temperature- 1200 °C and (d) 40 passes, solids wt %- 34.7 and sintering temperature- 1150 °C.

Microstructure / Layer Thickness

Figure 16 (a) and (b) show the SEI (at 10kV) of typical printed electrolyte, YSZ. The electrolyte appears dense and well sintered with grains about 2-4 µm. The thickness of electrolytes (not shown in fig.) ranged from 9-11 µm. Figure 17 a,b, and c shows the SEI (at 10kV) of cross sections of cells whose electrochemical performance is shown in Fig.2a, b, and c respectively. (Note that the magnification of image in (c) is different from that of (a) and (b)). The thicknesses of the cathode interlayer of all cells are in the range from 41 - 44 µm in thickness. The thickness of the LSM layer in cell (a) (40 print passes of LSM) is 50 µm and

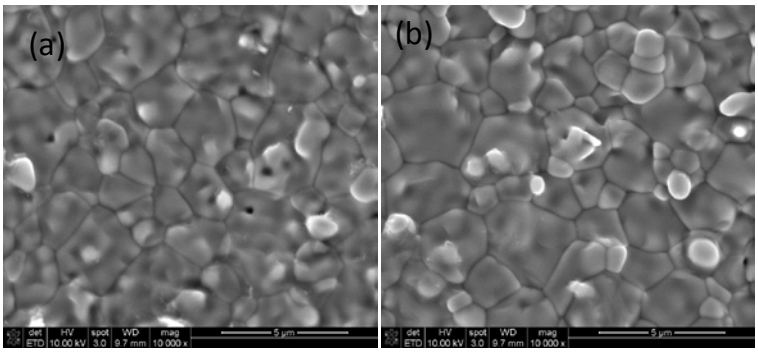

Figure 16. (a) and (b) Scanning electron microscopic image of surface of typical printed electrolyte, YSZ.

60 µm in cell (b) (60 print passes of LSM). The thickness of LSM layer in cell (c) is about 35 microns (cell with 17.4 wt% solids in LSM ink). Since the distinction of the different layers was not immediately clear at lower

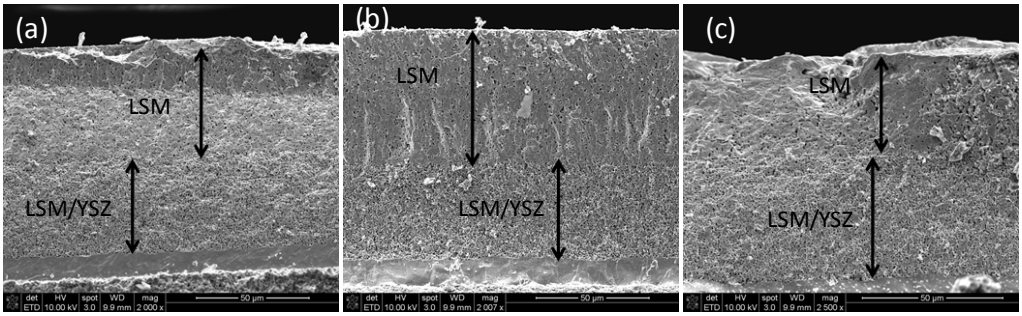

Figure 17: SE Image of cells with identically processed LSM/YSZ layer and varied LSM layer (a) 40 passes, solids wt%- 34.7 and sintering temperature- 1200 °C, (b) 60 passes, solids wt%- 34.7 and sintering temperature- 1200 °C, and (c) 40 passes, solids wt%- 17.4 and sintering temperature- 1200 °C.

magnification, several images were captured at many different magnifications to assess the thicknesses of layers shown here. Figure 18 a,b, and c shows images shown in fig. 17

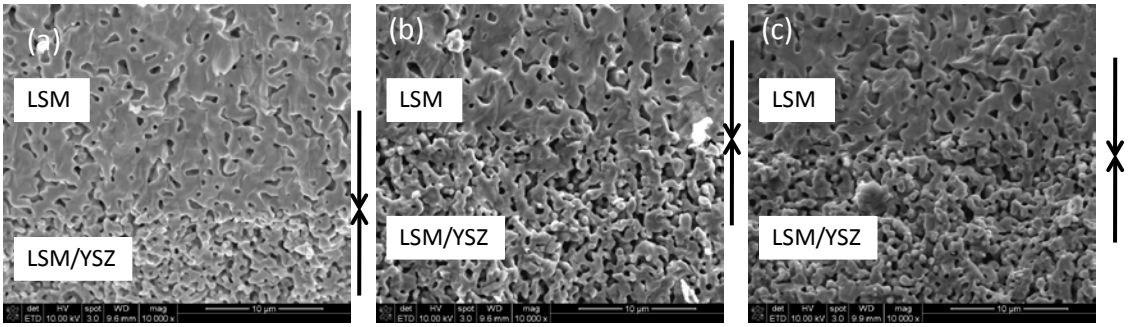

Figure 18: SE Image at higher magnification (of cross-sections shown in Fig.17), showing regions of LSM/YSZ layer and LSM layer.

only at a higher magnification. Portions of the interlayer, LSM/YSZ and current collection layer, LSM can be seen. LSM layer appears qualitatively to be less porous than the interlayer. This suggests that further manipulation of the layer porosity is required, and hence points to the possibility of much higher cell performance than is currently observed.

3.2.8 Miscellaneous printing: Fine line and large Area

In addition to the pneumatic atomizer for wide nozzle printing, the Optomec M^3D system is also equipped with an ultrasonic atomizer that can be used more specifically for fine line printing. The ultrasonic atomizer uses a piezoelectric transducer to atomize liquid source material. The transducer produces high-frequency pressure waves within the coupling fluid reservoir. These pressure waves are transmitted through the coupling fluid (typically water) and into the Atomizer Vial. Inside the vial, the pressure waves cause the ink or other liquid source material to be ejected from the surface of the fluid in the form of small droplets. The atomized droplets are then entrained in a gas stream and introduced into the deposition head. The ultrasonic Atomizer is best suited for materials with viscosity in the range of 0.7 – 30 mPa*s. Also, the suspended particles should be preferably on the order of 50 nm or less. The

ultrasonic atomizer printing was carried out using a standard Cabot silver ink. Figure 19 shows a pattern of silver lines 21 μm in width, printed using the ultrasonic atomizer using a 150 μm nozzle tip.

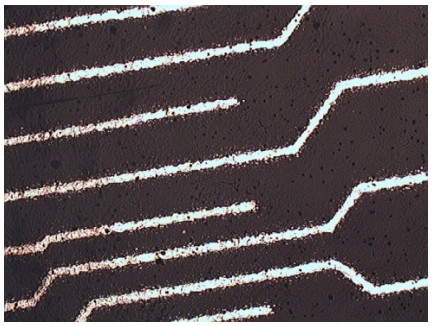

Figure 19: Silver metal pattern printed using the ultrasonic atomizer

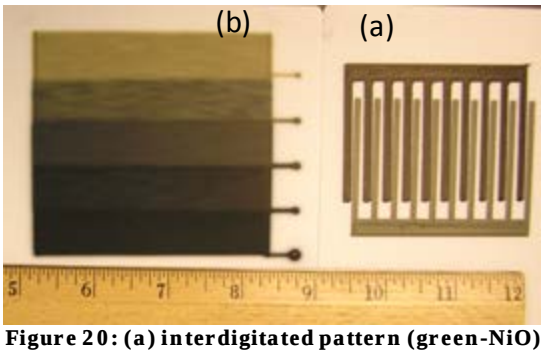

Figure 20: (a) interdigitated pattern (green-NiO) and (blck-LSM), (b) compositionally graded (in the plane of the paper) pattern.

Fig. 20 shows printing on larger areas using the pneumatic atomizer and wide nozzle (2.5 mm x 0.5 mm). Fig. 20 (a) is an interdigitated pattern (green- NiO ink, black-LSM ink) and pattern (b) shows gradation in the x-y plane. The bottom end (green region) is neat NiO and the top most region (pitch black) is neat LSM and the region in between has compositional gradation of NiO/LSM, with increasing amounts of LSM towards the darker region. The results of this work has been presented at technical conferences and published in peer reviewed journals. In addition, part of this work was the basis for a M.S. thesis.

3.3 Publications, Conference Presentations and Thesis work:

1) Sukeshini, A.M., Gardner, P., Jenkins, T., Reitz, T.L., and Miller, R.M., "Aerosol Jet Printing and Microstructure of SOFC Electrolyte and Cathode Layers", *ECS Transactions*, Vol. 35(1), "Solid Oxide Fuel Cells 12 (SOFC-XII)", 2011, 2151-2160.

2) Paul Gardner, M.S. thesis "Aerosol Jet Printing of LSCF cathode for SOFCs", Aug. 2011, Wright State University.

3) Loc P. Nguyen, Mary A Sukeshini, Ryan M. MillerMichael Rottmayer, and Thomas L. Reitz, "Effect of Ink Formulation and Sintering Temperature on the Microstructure of Aerosol Jet® Printed YSZ Electrolyte for Solid Oxide Fuel Cells," Annual Research Symposium, Ohio Aerospace Institute, Cleveland, April 08, 2011.

4) Sukeshini, A.M., Gardner, P., Jenkins, T., Reitz, T.L., and Miller, R.M., "Investigation of Aerosol Jet Deposition Parameters for printing SOFC layers", *Proceedings of the ASME 8th International Conference on Fuel Cell Science, Engineering and Technology*, vol. 1, pp 325-332 (2010).

5) Sukeshini, A.M., Gardner, P., Jenkins, T., Reitz, T.L., and Miller, R.M., Renn, M., and Ramahi, D., "Aerosol Jet Deposition for SOFC Fabrication," poster presentation at the 217 th Electrochemical Society Meeting, Vancouver, April 25-30, 2010.

4 Future Work

The in-house efforts will continue to focus on process development that will lead to high power dense fuel cells. While the current work has unambiguously demonstrated several unique features and advantages of aerosol jet printing not possible with traditional methods-high reproducibility of button SOFC performance, potential for producing combinatorial libraries of materials with a wide range of compositions and functional gradation, there are several technical challenges that need to be addressed. The layering effect of Ni and YSZ in the anode interlayer implies an improper mixing. But no layering effect is seen in the cathode interlayer (Figure 14). This implies a role of aerosol dynamics that is likely dependent on droplet size governing the mixing of phases. This observation warrants a more fundamental level of understanding of aerosol dynamics, mixing state and coagulation of droplets. Also, the relationship between aerosol dynamics and rheological properties of inks needs to be understood so that the inks can be tailored to enhance aerosol mixing of binary phases.

Through the current collaboration with Optomec Inc., it is expected that certain accessories for conformal printing will be delivered. On delivery of the accessories, process development work for printing components on non-planar SOFC substrates will be carried out. Tubular SOFCs have some advantages over the currently investigated planar configuration in that they have simpler seal requirements, and are also more robust having higher mechanical and thermal stability. The system start-up and shut down is faster compared to planar configurations.

4.1 Key Milestones

Optimization of Anode Functional Gradation:

- Baseline cell performance
    - compare the effect of printed interlayer with pasted to understand the electrochemical behavior
    - modify processing parameters
- Microstructural evaluation of composite phases and degree of mixing
- Iterate ink formulation, study dispersion stability

Intermediate Temperature Cathode Materials:

- Characterize cathode materials such as strontium doped lanthanum cobaltite ferrite and gadolinia doped ceria
    - formulate Ink , study rheology, and dispersion stability
    - establish print protocols
- Assess electrochemical performance

Demonstration of deposition on Tubular SOFC:

- Procure tubular anode support from commercial sources
- Using default YSZ ink formulation, deposit electrolyte layer

- Modify current printing protocol for YSZ for uniform coating on curved surfaces
- Determine layer thicknesses
- Examine layer microstructure

Protective coating for interconnects in stacks

- Ferritic steel with rare earth perovskite or spinel structures
    - formulate ink
    - establish print protocol
    - thermal treatment

All planned work will be performed in appropriate AFRL/RZPS facilities. Some work relating to scanning electron microscopy will be carried out at RXLM. The research work is normal or routine basic and applied scientific research confined to the laboratory and in compliance with all safety and environmental protocols and laws.

5 Conclusion

Research is ongoing to develop RZPS in-house expertise in the development of solid oxide fuel cells that have potential military application as field power generators, aircraft auxiliary power units (APUs) and primary power units for small unmanned air vehicles (S-UAV).

While considerable progress has been made in the scientific community at large, from the materials perspective, SOFC manufacturing methods currently available are limiting. Commonly used methods for fabricating the various cell components are based on wet ceramic processing techniques such as tape casting, screen printing, spray, spin and dip coating for thicker films in the mesoscale range or physical/chemical vapor deposition methods for films in the sub-micron to a few microns in thickness. These methods are not suited for mass manufacture due to limitations in either scale-up or cost. AFRL/RZPS has been collaborating with Optomec Inc., developing relevant processing methods to use aerosol jet printing, an additive manufacturing method developed by Optomec Inc. to deposit ceramic layers with suitable microstructures to function as electrode and electrolyte components in a SOFC. The process development work has involved ceramic ink formulation, establishing print protocols, materials processing, microstructural evaluation, device fabrication, and electrochemical testing of devices.

RZPS has successfully demonstrated the viability of the novel printing method as a suitable advanced manufacturing method for achieving highly reproducible multi-layered SOFC configurations. Through the current work, RZPS is not only making important contributions that address the Air Force needs, but is also playing a key role in furthering the potential commercialization of SOFC manufacturing technology.

6 References

1) 1. N. Minh, 'Ceramic Fuel-Cells,' *J. Am. Ceram. Soc*., **76**, 563 (1993).

2) 2. S. Singhal, "Advances in solid oxide fuel cell technology," *Solid State Ionics,* **135**[1-4], 305-313 (2000).

3) H.H. Dobbs, T. Krause, R. Kumar, and M. Krumpelt, Diesel-Fueled Solid Oxide Fuel Cell Auxiliary Power Units for Heavy-Duty Vehicle, *4th European Solid Oxide Fuel Cell Forum*, Lucerne, Switzerland (2000).

4) D.L. Daggett, S. Eelman, and G. Kristiansson, Fuel Cell APU for Commercial Aircraft, *AIAA Inter. Air and Space Symp. and Expo.*, Dayton, OH, AIAA 2003-2660, (2003).

5) 5. R.J. Braun, M. Gummalla, and J. Yamanis, System Architectures for Solid Oxide Fuel Cell-Based Auxiliary Power Units in Future Commercial Aircraft Applications, *J. Fuel Cell Sci and Tech.*, **6**,031015-1 – 031015-10 (2009).

6) F. Teitz, H.P. Buchkremer , Stover D, "Components manufacturing for solid oxide fuel cells*",* *Solid State Ionics*, **152-153,** 373-381 (2002).